IJME

Int. J. of Applied Mechanics and Engineering, 2025, vol.30, No.3, pp.75-86
DOI: 10.59441/ijame/207140

DESIGN OF EXPANDED METAL MESHES FOR GENERATION OF TURBULENCE IN SHELL-AND-TUBE HEAT EXCHANGERS FOR INDUSTRIAL APPLICATIONS

M. Garavaglia*, M. Rottoli, M. Mantegazza and F. Grisoni
Process and Thermal, Industry, Brembana&Rolle, ITALY
E-mail: mgaravaglia@brembanarolle.com

Control of turbulence through use of lattice meshes has been a main topic in fluid-dynamic literature since mid of last century. A specific class of lattice meshes, known as expanded metal meshes, EMS, has been proposed for baffles design in novel longitudinal flow heat exchanger technology for promotion of turbulence under limited pressure drops about two decades ago. Present investigation aims at developing a simple model for the design and optimization of suitable EMS geometry for its utilization as turbulence promoter in shell and tube heat exchangers for industrial applications. Novelty of approach relies on pressure drops based geometry design for improved functional product features.

Key words: industrial heat transfer, shell-and-tube-heat exchanger, expanded metal mesh, optimization of turbulence generation to pressure drops, method for designing optimal baffles for heat exchanger.

1. Introduction

Shell-and-tube heat exchangers are robust and reliable equipment for transferring heat between fluids, widely used in a multiplicity of services in the Process Industry. Accordingly, their geometry has been object of innumerable developments with the aim of optimizing performances, increasing competitiveness, and extending expected life [1]. Conventional layout is based on so called "segmental baffles", which proves effective in the majority of services but suffers of a few, yet notable, drawbacks, suggesting alternate design could be taken into consideration.

(a)  (b) 

Fig.1. (a) EMbaffle® layout. (b) Rod baffle layout.

Longitudinal flow layout emerged as a valuable alternate in the *90*s with proprietary Rod-baffle design [2] which replaces conventional baffles with rods disposed along a regular squared-grid (Fig.1a). Along the years, other geometries arose based on same principle. One of them is the patented EMbaffle design [3], which further develops Rod-baffle concept aiming at improving heat transfer performance, reducing fouling

* To whom correspondence should be addressed

deposition, increasing supporting capability of tube bundle and suppressing vibrations of fluid-dynamic and acoustic nature. EMbaffle makes use of a peculiar type of regular (i.e. lattice) mesh, named "expanded metal" (Fig.1b). Fluid-dynamics of lattice meshes has been object of extensive theoretical and experimental studies in the last eighty years (see [4] for extended review of relevant works). This paper aims at developing a model to optimize expanded metal grid used in longitudinal flow heat exchangers, as function of limited number of geometrical parameters, for attaining a closer control in resulting pressure drop and turbulence intensity.

2. Lattice meshes and turbulence

Lattice meshes have received considerable interest in the fluid-dynamics community due to several factors. Far downstream, a uniform lattice flows with high Reynolds number approximate isotropic homogeneous turbulence (Fig.2a); albeit inadequate from representing the majority of turbulent flows, isotropic homogeneity permits simpler investigation of the main physical phenomena of turbulence by providing some insights for useful generalization. Yet, lattice meshes have been used to control turbulence (either to promote and mitigate it), in several cases of practical interest [5, 6, 7].

About *20* mesh hydraulic diameters downstream the grid, turbulence assumes an isotropic homogeneous character [8]. Turbulent energy, at any points, is generated by Reynolds stresses at the expenses of the mean flow and finally dissipated as heat by viscous stresses. There is no direct energy transfer between Reynolds stresses and viscous stresses; large vortexes generated by Reynolds stresses are first transferred to smaller vortexes through an inertial mechanism (valid also for non-viscous flows). In this stage energy is conserved. Further on, energy starts dissipating through formation of vortexes of smaller and smaller size (Fig.2b), down to Kolmogorov scale; more detailed math about turbulence and vortexes can be found in [9].

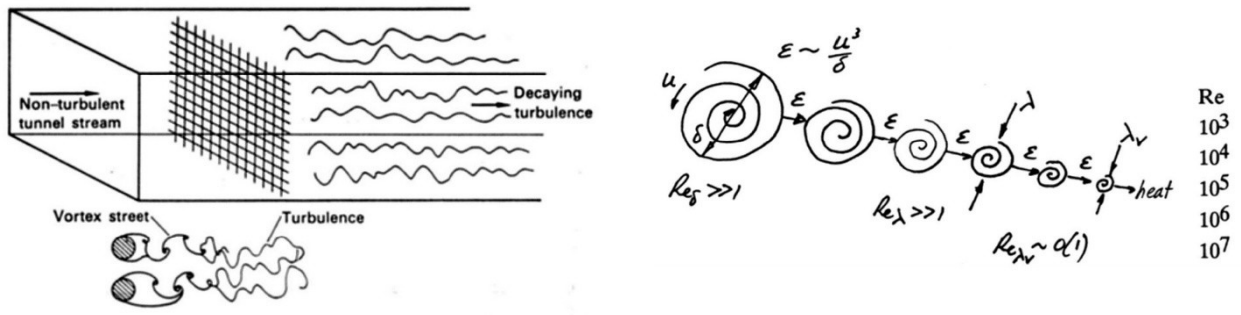

(a) (b)

Fig. 2. (a) Turbulence behind grids. (b) Scales of turbulence.

Mesh diameters for establishment of isotropic homogeneous turbulence may however have less significance in industrial applications whereas turbulence is voluntary generated to induce effects whom intensity has to be finely controlled. Here, it becomes pivotal to investigate the turbulent flow just downstream the lattice.

Bernoulli equation provides the rational for further investigations [10]:

$$\frac{\Delta p}{\rho V_0^2/2}+\left(\frac{V}{V_0}\right)^2+\left(\frac{v_x'}{V_0}\right)^2+\left(\frac{v_y'}{V_0}\right)^2+\left(\frac{v_z'}{V_0}\right)^2+\frac{\Delta h}{\rho V_0^2/2}=1. \tag{2.1}$$

Measurements conducted upon a regular mesh in the near range across it, result as per Fig.3.
A few considerations follow. While the different energy contributions tend to stabilize after *20* mesh diameters, our attention is focused in the region immediately before the mesh and just after. Upstream the mesh and immediately downstream, energy is transferred between kinetic component and pressure. Further on, pressure

does not recover entirely due to viscous dissipation, as quantified by the increase of internal energy: three main regions develop. In the first one (from *2* to *4* diameters), kinetic energy start diminishing while pressure recovers; no contribution of viscous dissipation appears. In the second one (from *4* to *12* diameters) kinetic energy and pressure proceeds the same way but internal energy start increasing.

In other words, flow is iso-entropic in the first region where total pressure is constant, while abrupt enlargement causes total pressure to fall and static pressure to rise. Finally, all contributions reach their equilibrium threshold.

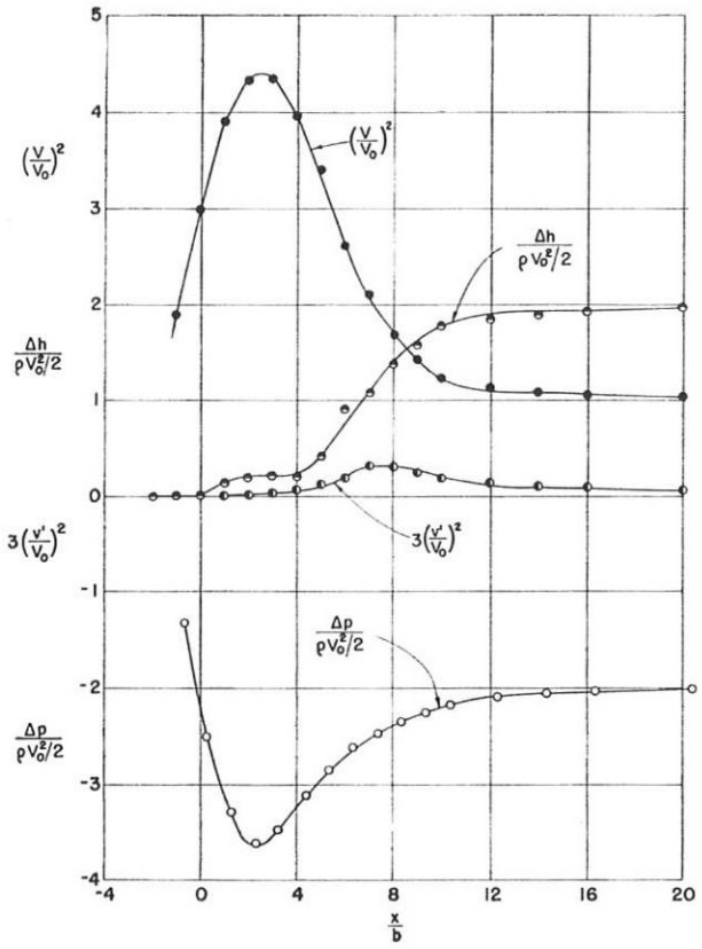

Fig.3. Turbulence across grids.

It can be noted that at $\frac{x}{b} = -4$ and at $\frac{x}{b} = 20$ sum of the terms equals one, as per Eq.(2.1).

By assuming that generation of vortexes occurs in the region between (-1) to $(+2)$ mesh diameters, the transfer of energy between large and medium-size eddies (inertial region) occurs in the region immediately after, up to *4* mesh diameters; further on dissipation proceeds in turbulence smoothing.

Pressure variation can be correlated to turbulence generation due to the lattice mesh by observing that integrating the |2.1| between the upstream section and the section of uniform velocity (Fig.4), it results

$$\frac{\Delta p|_{V_o}^{V_3}}{\rho V_0^2/2} + \left(1 + T_x^2 + T_y^2 + T_z^2\right) + \frac{\Delta h}{\rho V_0^2/2} = 1. \tag{2.2}$$

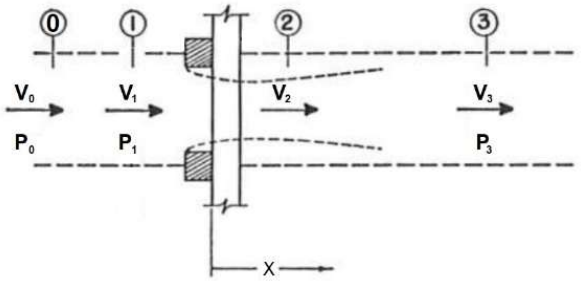

Fig.4. Turbulent stream in a channel.

Whereas the resulting flow does not show viscous effects, term $\Delta p\,|_{V_o}^{V_3}$ can be straightforwardly correlated with mesh geometry; *T* group gives contribute of the mesh to turbulence generation.

Therefore, pressure variation occurs due to change of geometry of the flow channel because of the mesh and the turbulence it generates. While pressure variation due to geometry effect is recovered, mesh induced turbulence will be fully dissipated, hence pressure drop across the mesh, which is part of pressure variation, would equal the contribute of the *T* group.

Pressure drop can be modeled through a term dependent on the $\frac{(1-\beta)^2}{\beta^2}$ group, being β the porosity of the mesh corrected by the coefficient of flow contraction. Named *K* the flow resistance coefficient, it results to be [4]:

$$\frac{\Delta p}{\rho V_0^{\,2}/2} = K = a\left(\frac{1}{\beta^2} - 1\right)^b \tag{2.3}$$

here and further on, Δp refers to pressure drop.

In general terms and for an incompressible flow *K* is a function of Reynolds number other than porosity [11, 12, 13]. By considering Reynolds number based on mesh wire diameter Re_d, *K* decreases with it until a limiting value of Re_d is reached; then *K* depends by porosity only. Notably, such a simplification occurs for high Reynolds numbers; in this region *a*, *b* in Eq.(2.3) depend just by mesh geometry.

3. Fluid-dynamics of lattice meshes.

Lattice meshes may have different shapes [14]. Expanded metal mesh (EMS), frequently used as filters of particulate in the automotive sector, deserves considerable interest for the plurality of potential applications it may address [15]. Researchers conducted in the last decade of the past century [16, 17] explore their behavior as turbulence promoters and highlight the typical flow resistance coefficient and turbulence intensity they give rise. Yet, they evidence the greater effectiveness of EMS, due to its inner structure, as "turbulence regulators" [18, 19, 20] when compared with more conventional types of meshes (e.g. square mesh arrays of wires/rods/bars, perforated plates, and others) [21, 22, 23, 24].

EMS geometry is mainly driven by production process (Fig.5). The plate of raw metal material is slit and expanded at same time by a cutter whose movement gives the cell its final shape; plate is then pushed forward for the generation of the next row of cells.

Cutter is designed for an assigned *cutting width*, *depth of slit* determines the height of the resulting cell, while *advancement* models its shape. Accordingly, EMS may be described by a set of geometrical parameters: *LWD*, *SWD*, *SW* (strand width) and *ST* (strand thickness) (Fig.6).

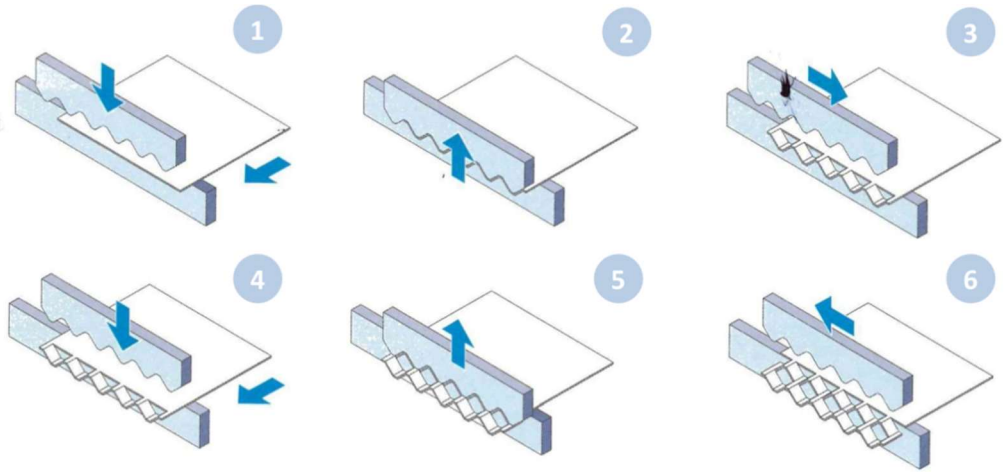

Fig. 5. Production process of an EMS.

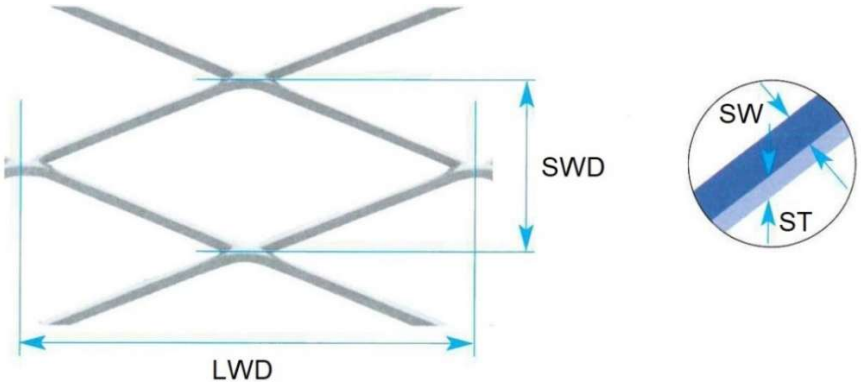

Fig.6. Geometry of an EMS.

Pinker and Herbert equation [11]:

$$K = f\left(Re_d\right)\frac{\sigma^2}{(1-\sigma)^2} \tag{3.1}$$

has been used to characterize pressure drops of various mesh geometries and to correlate K coefficient. Solidity σ is the reciprocal of porosity and represents the portion of the cell which opposes resistance to incident flow. Here $f\left(Re_d\right)$ is a function of Re_d, whose value is in the range $0.6-0.8$ for $Re_d > 40$ and here-on can be assumed constant.

Stream-wise turbulence intensity, T_x can be expressed through modified Frenkiel [25, 8] equation

$$T_x = 7.0\left(\frac{ST}{SWD}\right)^{0.82}\left(\frac{x}{d}\right)^{-5/7}, \tag{3.2}$$

applicable for $x/d > 20$ mesh diameters, whereas x/d is the distance downstream the mesh location.

While Eq.(3.1) and Eq.(3.2) allow straightforward prediction of non-dimensional pressure drop and turbulence intensity for any EMS, their general formulation is not functional to the optimization of cell geometry.

Under the hypothesis that $SW^2 \ll SWD \cdot LWD$, which is generally verified, solidity can be expressed as a function of angle α, formed by the side of the cell and *LWD* (Fig.7)

$$\sigma = \frac{1}{2L} SW \frac{\sin\alpha + \cos\alpha}{\sin\alpha \cos\alpha}. \tag{3.3}$$

Above provides a more productive relation; indeed, as it may be shown, derivate of Eq.(3.1) + Eq.(3.2) results in:

$$\frac{\partial K}{\partial \alpha} = \frac{\partial K}{\partial \sigma}\frac{\partial \sigma}{\partial \alpha} = \frac{1}{2L} f(\sigma) SW \left(\frac{\sin\alpha}{\cos^2\alpha} - \frac{\cos\alpha}{\sin^2\alpha} \right) \tag{3.4}$$

whereas $f(\sigma)$ is an ever-positive function and the trigonometric group has a zero, which is a *K*-minimum, for $\alpha = \pi/4$.

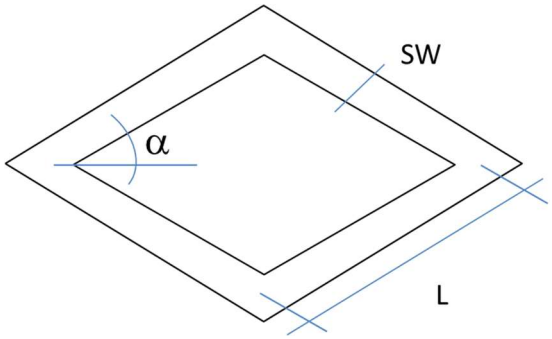

Fig.7. Geometry of an EMS cell.

Under the above, pressure drop shows therefore a minimum for square-cell design.

Unfortunately, Eq.(3.2) does not allow the same treatment; here Eq.(2.3) can assist by observing that *T* group collapses into $3T_x^2$ under homogeneous isotropy condition:

$$T_x|_{max} = \frac{\sqrt{3}}{3} K^{0.5}. \tag{3.5}$$

Validity of Eq.(3.5)| had to be checked before being used in direct calculation of stream-wise turbulence intensity.

As it may be expected, maximum intensity is related to pressure drop, hence the square shaped cell is either suffering less fluid-dynamic losses and reduced turbulence.

4. Turbulence in longitudinal heat transfer flow

Generation of turbulence for promotion of heat transfer is an interesting application where EMS prove. Here each cell in a mesh embraces one heat exchanging tube (Fig.8), while providing room for flow of a fluid between the cell and the outer perimeter of the tube (shell-side).

Flow resistance coefficient, for infinite tube length, has been modeled [27, 28] as:

$$K = be^{c\left(-\frac{A_b}{A_s}\right)} \tag{4.1}$$

whereas A_b can be expressed as function of the mesh solidity σ_t.

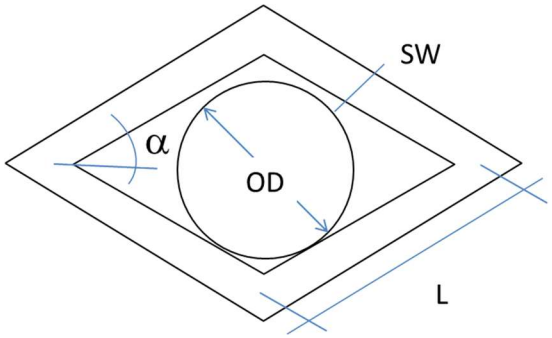

Fig. 8. Geometry of an EMS cell embedding a tube.

As in case of no-tube-in-cell, flow resistance coefficient can be correlated with geometry of the cell

$$\sigma_t = \sigma + \frac{\pi}{16}\left(\frac{OD}{L}\right)^2 \frac{1}{\sin\alpha\cos\alpha}. \tag{4.2}$$

By observing that

$$\frac{\partial K}{\partial \alpha} = \frac{\partial K}{\partial A_b}\frac{\partial A_b}{\partial \sigma_t}\frac{\partial \sigma_t}{\partial \alpha} = de^{c\left(-\frac{A_b}{A_s}\right)} g(\alpha), \tag{4.3a}$$

$$g(\alpha) = \frac{1}{2L} SW\left(\frac{\sin\alpha}{\cos^2\alpha} - \frac{\cos\alpha}{\sin^2\alpha}\right) - \frac{\pi}{4}\left(\frac{OD}{L}\right)^2 \frac{\cos 2\alpha}{\sin^2 2\alpha}. \tag{4.3b}$$

The above is valid for any L and SW not dependent by α, both conditions being generally verified.

Function $g(\alpha)$ has zero for $\alpha = \pi/4$, regardless the value of OD/L. Accordingly, K reaches its own minimum; it descends that such a configuration minimizes the pressure drop and, as it may be expected, the turbulence intensity for square-cell design as in no-tube-in-cell layout.

Moving forward, a tool for designing an effective mesh is described.

Idea is to calculate the new mesh geometry on the basis of an initial value of angle α, then solidity is calculated through Eq.(4.2) + Eq.(3.3). Flow resistance coefficient is derived by Eq.(4.1) and relating turbulence by Eq.(3.2) at any location downstream. Calculation is replicated for values of angle α and the K-curve is drawn; ref. to next chapter 5 for operational details.

Validation of the method is required to assess its quality and limits of utilization.

A conceptual test bench has been arranged for preliminary validation of commercial EMS; yet further investigation is required to fully assess the proposed methodology. Shell-and-tube heat exchanger, whose main mechanical features are reported in Tab.1a, has been tested with air at shell-side under process conditions and thermo-physical properties are reported in Tab.1b.

A set of commercial EMS has been successively replaced inside the heat exchanger.

Each EMS can be defined through three main parameters: *SWD*, *LWD* and *SW*, having set the thickness of the raw material plate; average *SW* is $2.38\ mm$. For EMS can be installed regardless its orientation, rotated geometry has been considered and indicated with '*90*' addition.

Table 1. (a) Geometry of Heat Exchanger. (b) Process properties of the test.

(a) Geometry of Heat Exchanger		
N tubes	*60-74*	
L tube	*6000*	*mm*
OD tube	*15.875*	*mm*
OTL bundle	*195*	*mm*
D inner shell	*211.5*	*mm*
D outer ring	*208*	*mm*
D inner ring	*198*	*mm*
N baffles	*29*	

(b) Thermo-physical Properties		
ρ	*1.86*	kg/m^3
c_p	*1006.1*	*J/kgK*
k	*0.0307*	*W/mK*
μ	*2.11e-5*	Ns/m^2
Process Data		
T	*113*	*C*
P	*1*	*barg*

Calculation of *K* for individual EMS based on Eq.(4.1) is reported in Fig.9; prediction curve K_{th}, built on Eq.(4.1) + Eq.(4.2), is superposed.
Comparison shows fair prediction capability of the proposed formula with exception of one point (ref. $5/8"H$) whose apparent solidity is higher than predicted.

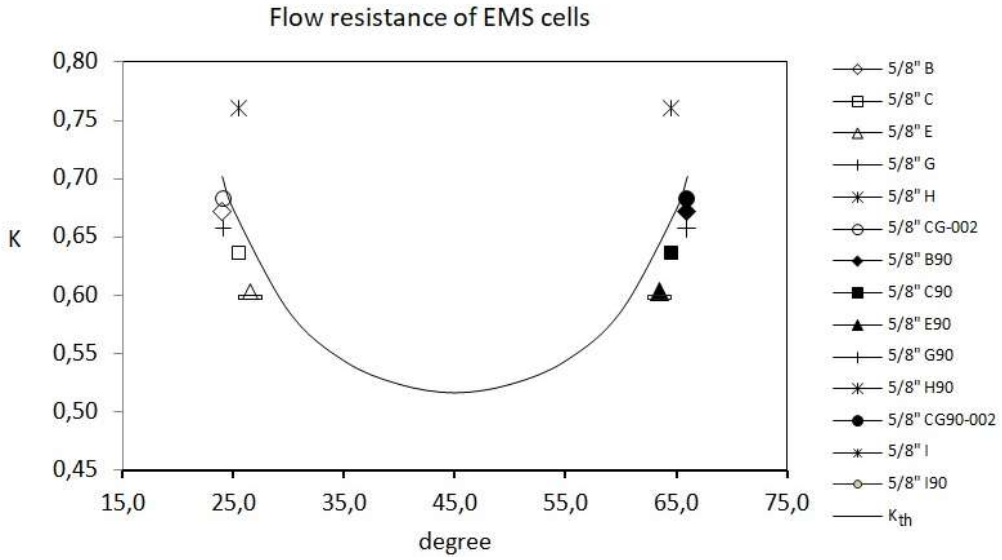

Fig. 9. Flow resistance of an EMS cell.

Influence of *SW* and *L* can be envisaged for variations in *SW* and *L* respectively.

In Fig.10 K_2 and K_1 are calculated for *SW* equal to *1.5 mm* and *4.0 mm* respectively. Here *L* is equal to *24.5 mm*, the value of the set of EMS utilized. While small *SW* values generate lower pressure drop, choice of α has minor impact over design: indeed, variation of *K* in a large range around *45 deg* is almost negligible. The opposite is true for large *SW*, especially close to the limit angles *20 deg* and *80 deg* where turbulence intensity is expected to be substantial.

Generalization of the above can be obtained by Eq.(4.3b) expressing the rate of change of solidity σ with angle α; Fig.11 provides graphical representation for two configurations: high solidity (σ'), based on $SW = 4.0\,mm$, $L = 22.5\,mm$ and low solidity (σ), based on $SW = 1.5\,mm$, $L = 26.0\,mm$.

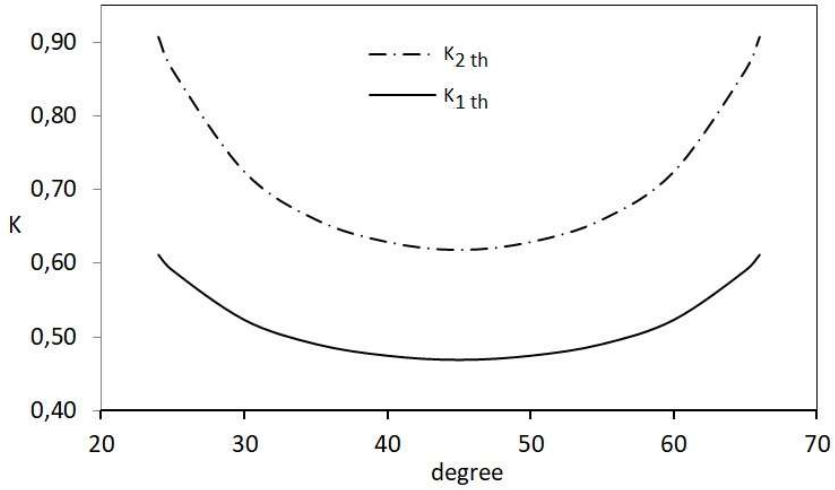

Fig.10. Sensitivity of the model respect to SW.

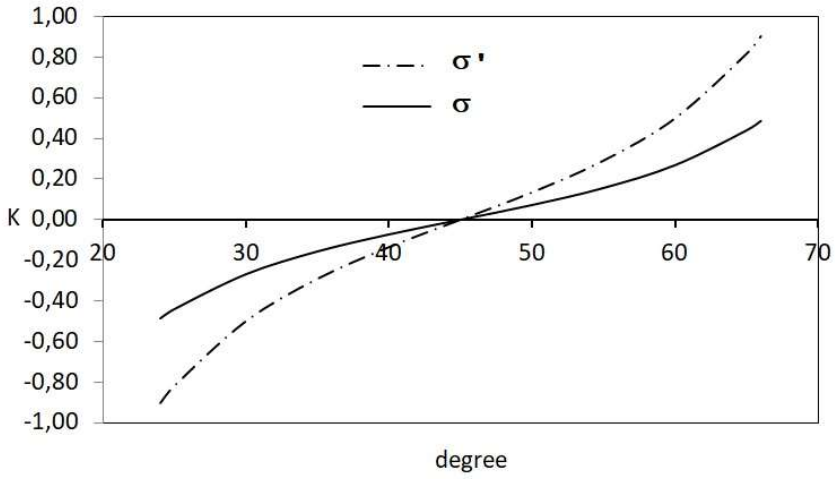

Fig.11. Sensitivity of the model for high and low solidity.

Rate of change of 'high solidity' is higher than for 'low solidity' and it is specifically true for small values of the angle (close to zero and close to *90 deg*).

The above provides a useful guide for evaluation of geometry suitable for purpose; moreover it suggests some hints for future investigations.

5. Design of EMS for industrial applications

Design process is outlined below

- selection of thickness of raw material plate (*ST*), which is usually in the range *1.5 mm* to *2.5 mm* for *OD = 5 / 8*" to *1*" and results by mechanical resistance considerations.
- selection of *SW*, usually in the range *1.5 mm* to *4.0 mm* for same *OD*s; higher *SW* increase solidity of resulting mesh but larger values may generate uncontrolled turbulence effects.

- application of Eq.(3.3) + Eq.(4.2) for calculation of solidity $\sigma = \sigma(\alpha)$ and final design parameters: *SWD*, *LWD*.
- application of Eq.(4.1) for calculation of flow resistance coefficient *K*.
- choice of suitable σ based on project requirements, which can be declined in terms of low pressure drops, i.e. small *K* and close-to-square-cell design or increased turbulence intensity, which means larger *K* and small angle design.
- as a general note, smaller angle (e.g. less than *20 deg* and large than *70 deg*) and too much irregular shapes should be avoided; yet out-of-shape material resulting from production process has major influence over small angle design, by obstructing portions of free flow area and increasing solidity as well.

6. Conclusions

A simplified calculation method for designing EMS-based baffles for longitudinal flow heat exchangers has been presented and preliminarily validated on basis of available commercial geometries. Method, whom applicability had to be further investigated, may be useful for anticipating EMS geometry based on pressure drop requirements for the specific application. Accordingly, Designer, within project requisitions, may decide to design a mesh in the direction of attaining lower pressure drop and reduced turbulence or to accept larger pressure drop for improving turbulence intensity. Proposed method embeds in its own formulation the optimization of turbulence generation (in terms of resulting pressure drops) and, in principle, does not require further verification of the resulting EMS from design.

In heat transfer applications, decision regarding level of optimization is related to the additional amount of heat that improved turbulence may generate; correlation of heat transfer and pressure drop and optimization of their ratio will therefore be the natural object of ensuing contribute.

Nomenclature

A_b – free flow area across the mesh

A_s – shell side flow area at mesh location

K – flow resistance coefficient

Re – Reynolds number

T – turbulence intensity

V_0 – upstream undisturbed velocity of the flow

V_2 – velocity at the contracted section downstream the mesh

V_3 – uniform downstream velocity

v' – turbulent velocities

x / d – distance downstream the mesh

Δh – variation of internal energy $h - h_0$

Δp – pressure variation $p - p_0$

ρ – fluid density

σ – solidity

References

[1] Thulukkanam K. (2013): *Heat Exchanger Design Handbook, 2nd Edition*.– CRC Press, Boca Raton, FL/US. DOI/10.1201/b14877.

[2] Gentry C.C. (1994): *Rod-Baffle Heat Exchanger Design and Applications*.– Int. Heat Transfer Conference 10, pp.137-142, DOI: 10.1615/IHTC10.5180.

[3] Rottoli M., Odry T., Agazzi D.and Notarbartolo E. (2016): *EMbaffle® Heat Exchanger Technology - Innovative Heat Exchangers*.– Springer Nature, Heidelberg, Germany, pp.341-361, DOI/10.1007/978-3-319-71641-1_11.

[4] Roach P.E. (1986): *The generation of nearly isotropic turbulence by means of grids*.– Int. J. Heat Fluid Flow, Amsterdam the Netherlands, vol.8 No.2, pp.82-92, DOI/10.1016/0142-727X(87)90001-4.

[5] Laws E.M. and Liversey J.L. (1978): *Flow through screens*.– Ann. Rev. Fluid Mechanics, San Mateo CA/US, vol.10, pp.247-266, DOI/10.1146/annurev.fl.10.010178.001335.

[6] Schubauer G.B., Spangenberg W.G. and Klebanoff P.S. (1950): *Aerodynamic Characteristics of Damping Screens*.– NACA TN 2001. DOI not available.

[7] Corrsin S. (1942): *Decay of Turbulence behind Three Similar Grids*. – M.Sc. Engineering Thesis, CalTech, Pasadena, CS/US. DOI:10.7907/GXRW-6609.

[8] Frenkiel F.N. (1948): *The decay of isotropic turbulence*.– J. Applied Mechanics, New York, NY/US, vol.15, No.4, pp.311-321, DOI/10.1115/1.4009853.

[9] Batchelor G.K. (1967): *An Introduction to Fluid Dynamics* – Cambridge University Press, Cambridge, UK, DOI /10.1017/CBO9780511800955.

[10] Baines W.D. and Peterson E.G. (1951): *An investigation of flow through screens*.– Transaction ASME, New York, NY/US, vol.73, pp.467-480, DOI:10.1115/1.4016280.

[11] Pinker R.A. and Herbert M.V.(1967): *Pressure loss associated with compressible flow through square-mesh wire gauzes*.– J. Mechanical Engineering Science, Thousand Oaks CA/US, vol.9, No.1, pp.11-23, DOI:10.1243/JMES_JOUR_1967_009_004_02.

[12] Iwaniszyn M., Sindera K., Gancarczyk A., Leszczyński B., Korpyś M., Suwak M., Kołodziej A. and Jodłowski P.J. (2022): *Characterization of fluid flow and heat transfer of expanded metal meshes for catalytic processes*.– Energies J., https://www.mdpi.com/journal/energies, DOI/10.3390/en15228437.

[13] Shirao P., Jagtap H., Magade P., Gadhave P. and Kamble D. (2024): *Thermo-hydraulic analysis of fluid flowing through circular pipes with wire mesh inserts having varied mesh porosities*.– Earth and Environmental Science - IOP Conference Series, DOI:10.1088/1755-1315/1285/1/012028.

[14] Smith D., Graciano C. and Martinez G. (2021): *Expanded metal: a review of manufacturing, applications and structural performance*.– Thin Walled Structures J., vol.10, Elsevier, DOI/10.1016/j.tws.2020.107371.

[15] Ghaemi S. (2020): *Passive and active control of turbulent flows*.– Physics of Fluids, vol.32, DOI/10.1063/5.0022548.

[16] Oshinowo O.M. (1997): *Flow modifying Screens in Turbulent Flows*.– M.Sc. Thesis, Toronto, DOI not available.

[17] Oshinowo L. (1999): *Two dimensional flow deflection screen model*.– J. Chemical Engineering, Hoboken NJ/US, vol.77, pp.122-126, DOI/10.1002/cjce.5450770120.

[18] Grant H.L. and Nisbet I.C.T. (1957): *The inhomogeneity of grid turbulence*.– J. Fluid Mechanics, Cambridge, UK, vol.2 No.3, pp.263-272, DOI/10.1017/S0022112057000117.

[19] Grzelak J. and Wiercinski Z. (2015): *The decay power law in turbulence generated by grids*.– Trans. Inst. Fluid Flow Machinery, Gdansk, Poland, vol.130, pp.93-107.

[20] Uberoi M.S. and Wallis S. (1967): *Effect of grid geometry on turbulence decay*.– The Physics of Fluid, Melville NY/US, vol.10, pp.1216-1224, DOI/10.1063/1.1762265.

[21] Inagaki A., Ishii D., Asaji T., Nakamura T., Watanabe N., Kikuchi T. and Takahashi K. (2020): *Effect of blowdown wind tunnel inlet on the mainstream turbulence intensity*.– Transactions on Gigaku, DOI:10.34468/GIGAKU.7.1_07006-1.

[22] Nie L.X., Yin Y., Yan L.Y. and Zhou S.W. (2021): *Pressure drops measurements and simulations for the protective mesh screen before the gas turbine compressor*.– Proceedings of the 2nd International Conference on Green Energy, Environment and Sustainable Development (GEESD2021), DOI:10.3233/ATDE210277.

[23] Jafari A., Emes M., Cazzolato B., Ghanadi F. and Arjomandi M. (2021): *Wire mesh fences for manipulation of turbulence energy spectrum*.– Experiments in Fluids J., vol.62, No.30, DOI/10.1007/s00348-021-03133-7.

[24] Wang Y., Yang G., Huang Y., Huang Y., Zhuan R. and Wu J. (2021): *Analytical model of flow through screen pressure drop for metal wire screens considering the effects of pore structures*.– Chemical Engineering Science J., vol.229, DOI/10.1016/j.ces.2020.116037.

[25] Oshinowo L. and Kuhn D.C.S. (2000): *Turbulence decay behind expanded metal screens*.– The Canadian J. Chemical Engineering, Hoboken NJ/US, vol.78, pp.1032-1039, DOI/10.1002/cjce.5450780602.

[26] O'Neill F.G. and Breddermann K. (2024): *The contribution of mesh opening angle to the drag of netting panels*.– Ocean Engineering J. vol.305, Elsevier, DOI/10.1016/j.oceaneng.2024.117959.

[27] Perrone F., Brignone, Micali G. and Rottoli M. (2014): *Grid geometry effects on pressure drops and heat transfer in an EMbaffle® heat exchanger*.– International CAE Conference 2014, Verona, Italy. DOI not available.

[28] Garavaglia M., Grisoni F., Mantegazza M. and Rottoli M. (2023): *Advanced shell and tube longitudinal flow technology for improved performances in the process industry*.– Heat Transfer, Advances in Fundamentals and Applications, InTech Open, Rijeka, Croatia, DOI: 10.5772/intechopen.113132.

Received: January 15, 2025
Revised: June 14, 2025